



1                   **Ionospheric Pc1 waves during a storm recovery phase**  
2   **observed by CSES**

3   Xiaochen Gou<sup>1</sup>, Lei Li<sup>1\*</sup>, Yiteng Zhang<sup>1\*</sup>, Bin Zhou<sup>1</sup>, Yongyong Feng<sup>1</sup>, Bingjun Cheng<sup>1</sup>  
4   Ji Liu<sup>1</sup>, ZhiMa Zeren<sup>2</sup>, Xuhui Shen<sup>2</sup>

5  
6   <sup>1</sup>State Key Laboratory of Space Weather, National Space Science Center, Chinese  
7   Academy of Sciences, Beijing 100190, China;

8   <sup>2</sup>Institute of Crustal Dynamic, China Earthquake Administration, Beijing 100029, China;  
9

10   **Abstract**

11   During the storm recovery phase on August 27, 2018, the China Seismo-  
12   Electromagnetic Satellite (CSES) detected Pc1 wave activities both in the Northern and  
13   Southern hemispheres in the high latitude post-midnight ionosphere with a central  
14   frequency about 2 Hz. Meanwhile, the typical Pc1 waves were simultaneously  
15   observed by the Sodankylä Geophysical Observatory (SGO) stations on the ground for  
16   several hours. In this paper, we study the propagation characteristics and possible  
17   source regions of those waves. Firstly, we find that the satellites observed Pc1 waves  
18   exhibit mixed polarization and the wave normal is almost parallel with the background  
19   magnetic field. The field-aligned Poynting fluxes point downward in both hemispheres,  
20   implying the satellites are close to the wave injection regions in the ionosphere at  
21   about  $L=3$ . Furthermore, we also find that the estimated position of the plasmopause  
22   calculated by models is almost at  $L=3$ . Therefore, we suggest the possible sources of  
23   waves are near the plasmopause, which is consistent with previous studies that the  
24   outward expansion of the plasmasphere into the ring current during the recovery  
25   phase of geomagnetic storms may generate electromagnetic ion cyclotron (EMIC)  
26   waves and then these EMIC waves propagate along the background magnetic field  
27   northward and southward to the ionosphere at about  $L=3$ . Additionally, the ground  
28   station data show that Pc1 wave power attenuates with increasing distance from  $L=3$ ,  
29   supporting the idea that CSES observes the wave activities near the injection region.  
30   The observations are unique in that the Pc1 waves are observed in the ionosphere in  
31   nearly conjugate regions, where transvers Alfvén waves propagate down into the  
32   ionosphere.

33  
34   **1 Introduction**

35   Electromagnetic ion cyclotron (EMIC) waves are in the typical frequency range of 0.1–  
36   5Hz which corresponds to Pc1 pulsations on the ground. Generally, in the



37 magnetosphere, EMIC wave can be excited by cyclotron instability of hot ions (1-100  
38 keV) with temperature anisotropy ( $T_{\perp} > T_{\parallel}$ ) near the Earth's magnetic equator,  
39 particularly, in the region with large plasma density and weak magnetic field, such as  
40 the plasmopause, ring current and plasma sheet [Cornwall et al., 1965; Erlandson et  
41 al., 1993; Horne and Thorne, 1993; Anderson et al., 1996; Lin et al., 2014]. Previous  
42 studies indicate that hot ion temperature anisotropy ( $T_{\perp} > T_{\parallel}$ ) near the Earth's magnetic  
43 equator can be caused by several possible mechanisms, such as plasmopause  
44 expanding into ring current region during storm recovery phase [Wentworth, 1964;  
45 Russell & Thorne, 1970], mid-energy ions penetrating into the ring current region from  
46 the plasma sheet [Bossen et al., 1976], the solar wind dynamic pressure enhancement  
47 or the magnetosphere compression [Olson & Lee, 1983; Anderson & Hamilton, 1993;  
48 McCollough et al., 2010; Usanova et al. 2012]. Statistical results show that EMIC waves  
49 are associated with magnetic activities and have a peak occurrence during the storm  
50 recovery phase [Wentworth, 1964; Erlandson & Ukhorskiy, 2001; Bortnik et al., 2008].

51

52 Generally, EMIC waves are excited at or near the Earth's magnetic equator, and then  
53 propagate along the background magnetic field toward the high latitude region, can  
54 penetrate into the upper ionosphere under certain conditions. The left-hand polarized  
55 (LHP) Alfvén waves incident from the magnetosphere can couple to the right-hand  
56 polarized (RHP) compressional, isotropic waves in the ionosphere by the anisotropic  
57 ionospheric Hall currents [Fraser et al., 1975a, 1975b; Fujita and Tamao 1988]. Since  
58 the wavelength of EMIC waves with frequency about 1Hz is comparable with the scale  
59 size of the ionospheric minimum in the Alfvén speed, they can be trapped and ducted  
60 in this region of low Alfvén speed [Lysak et al., 1999]. Thus, the EMIC waves can be  
61 observed both at the low earth orbit (LEO) and on the ground as Pc1 geomagnetic  
62 pulsations with different characteristics.

63

64 At ionospheric altitudes, satellite observations of Pc1 waves are usually provided by  
65 the onboard magnetometers. MAGAT observed Pc1 waves at an ionospheric altitude  
66 of 350-550km, with both LH and RH polarizations in a latitudinally narrow (<100 km)  
67 region [Iyemori and Hayashi, 1989]. In recent years, with the development of LEO  
68 satellites, various statistical studies of EMIC waves have been carried out to reveal the  
69 global propagation characteristics, spatial distribution, and geomagnetic dependence  
70 of Pc1 waves. According to the statistical analysis of CHAMP satellite data during one  
71 solar cycle, Park et al. [2013] found that Pc1 waves are mostly linearly polarized, having  
72 a peak occurrence at subauroral latitudes, and weakly dependence on the magnetic  
73 activity and the solar wind velocity. The SWARM data show a peak occurrence rate of  
74 Pc1 waves at middle latitude including sub-auroral zone. Moreover, these waves are



75 linear polarization dominated, propagating oblique to the background magnetic field,  
76 preferable to occur during late recovery phase of the storm [Kim et al. 2018a].

77

78 In this paper, we report a Pc1 wave event observed by the China Seismo-  
79 Electromagnetic Satellite (CSES), as well as the SWARM satellite. Based on both electric  
80 and magnetic field measurements, we study the propagation characteristics and  
81 possible source regions of those Pc1 waves occurring at high latitude in the Northern  
82 and Southern hemisphere ionosphere during the recovery phase of the geomagnetic  
83 storm on 25-28 August 2018.

84

## 85 **2 Data sources**

86 The China Seismo-Electromagnetic Satellite (CSES) was launched on February 2, 2018,  
87 into a sun-synchronous circular orbit at an altitude of 507 km with an inclination angle  
88 of 97.4°. The local time of the descending node is 14:00. We use the magnetic field  
89 data from the High Precision Magnetometer (HPM) and the electric field data from the  
90 Electric Field Detector (EFD) onboard CSES. HPM includes two three-components  
91 fluxgate sensors to collect vector magnetic field data with a sampling rate of 60Hz, and  
92 the noise of the sensors are less than 0.02nT /VHz @1 Hz [Zhou et al., 2018; 2019].  
93 EFD consists of four spherical sensors, which can realize three-components electric  
94 field detection at a broad frequency range from DC to 3.5MHz, in which the ULF band  
95 provides 125Hz sampled waveform signal [Huang et al., 2018]. SWARM was launched  
96 on November 22, 2013, which has three satellites at altitudes of 450 – 550 km with an  
97 inclination angle of 88°. In addition, we also use the geomagnetic data from Sodankylä  
98 Geophysical Observatory (SGO) stations, the solar wind data of OMNI from CDA Web  
99 and Dst index from WDC Web.

100

## 101 **3 Observations**

102 Figure 1 shows the variation of solar wind parameters and the geomagnetic index  
103 during the Pc 1 wave event in this study. The Dst index, interplanetary magnetic field,  
104 solar wind speed and solar wind dynamic pressure from Aug. 25 to 29, 2018 are shown  
105 from top to bottom. It can be seen that during the magnetic storm, the Dst index  
106 decreased to -170 nT at 8:00 26 August. On the days from 27 to 28 August, the  
107 interplanetary magnetic field (IMF) was northward, Dst experienced a minor increase.  
108 The Pc1 waves were observed by CSES and SWARM between UTC 22:50 – 23:30  
109 (marked by the black line in Figure 1) in the magnetic storm recovery phase on Aug.  
110 27, 2018.

111



### 112 **3.1 Spatial-temporal characteristics of Pc1 waves**

113

114 On Aug. 27, 2018, CSES and SWARM-A satellites passed through the ionospheric Pc1  
115 wave regions for three times, in the Northern and Southern hemispheres, marked by  
116 squares (CSES) and triangles (Swarm) in Figure 2. Firstly, at around UTC 23:00 (local  
117 time about 02:06 to 02:34), SWARM-A and CSES satellites were located at geomagnetic  
118 latitude about  $56^{\circ}$  S~ $53^{\circ}$  S, at  $L$  shell region about 3.0 ~ 3.4, with a distance about  
119 300km apart, both successively observed Pc1 waves in the Southern hemisphere, as  
120 shown in Figure 2. SWARM-A observed the Pc1 waves at about UTC 22:50 (QD-LAT= $56^{\circ}$   
121 S,  $L=3.4$ ) about 10 minutes before CSES, with a maximum amplitude about 12 nT and  
122 a central frequency about 2 Hz, lasting for 1 minute, as shown in Figure 3. Then, CSES  
123 observed the Pc1 wave at UTC 23:02 (QD-LAT= $54^{\circ}$ S,  $L=3.1$ ) by the magnetometer HPM  
124 (shown in Figure 4), with a maximum amplitude about 1.5 nT and a central frequency  
125 about 2 Hz, lasting a minute and a half. Thereafter, at about UTC 23:30 (local time  
126 about 01:27 to 01:22), the CSES flew away to the Northern hemisphere, passing  
127 through the Pc1 wave region again at geomagnetic latitudes about  $54^{\circ}$  N,  $L$  values  
128 about 3.1. As shown in Figure 5, the maximum amplitude is about 10 nT and the central  
129 frequency is about 2 Hz, with a duration about 1 minute. Around this time, since the  
130 SWARM satellite was about 6000 km northeast of the CSES satellite, no Pc1 waves  
131 were observed by SWARM.

132

133 At the same time, the typical Pc1 waves were also observed by the SGO stations on  
134 the ground for several hours. As shown in Figure 6, from UTC 22:00 to 24:00, SGO  
135 stations recorded continuous pulsations with a central frequency of about 2-3 Hz. In  
136 Figure 6, from top to bottom are the observations from SGO stations: Sodankylä (SOD;  
137  $L = 5.3$ ,  $64.3^{\circ}$ N,  $105.6^{\circ}$ E, QD), Oulu (OUL;  $L = 4.5$ ,  $61.9^{\circ}$ N,  $104.1^{\circ}$ E, QD), and Nurmijärvi  
138 (NUR;  $L = 3.4$ ,  $57.1^{\circ}$ N,  $101.2^{\circ}$ E, QD) from ~21:00 to 24:00 UT. The wave power of Pc1  
139 pulsations increases monotonically with the decrease of  $L$  shell values of SGO stations,  
140 with the maximum power at NUR station, which is close to the region where CSES  
141 observed Pc1 in the Northern hemisphere. Because of the ducting effect of Pc1 waves  
142 in the ionospheric waveguide, Pc1 waves are likely to be seen at a long distance away  
143 from the source region [e.g., Fujita and Taobao, 1988; Kim et al., 2010]. Since the  
144 boundary of the waveguide is not a perfect conductor, some absorption may happen  
145 when waves propagate in the waveguide, resulting in attenuation of the wave power.  
146 So, comparing the wave power observed by different ground stations, it is possible to  
147 infer the probable location of the wave source. Therefore, in our case, we suggest that  
148 the injection source region of the Pc1 waves in the Northern hemisphere should be  
149 near (QD-LAT= $54 - 56^{\circ}$ N,  $L \sim 3.3$ ), where CSES and NUR observed the pulsations, and



150 after incidence on the ionosphere, the waves were ducted toward northeast, observed  
151 by the ground stations located at higher latitudes.

152

### 153 **3.2 Propagation characteristics of Pc1 waves**

154 Wave polarization is another property that provides information on the wave source  
155 and spatial characteristics of wave propagation. According to theoretical studies, the  
156 incident LPH Alfvén waves in the ionosphere can gradually change to RHP as the waves  
157 propagate in the ionosphere away from the injection region [e.g., Fujita and Taoumao  
158 1986]. Close to the injection region, the polarization pattern is usually complex,  
159 because the waves near the injection source are combined with incident waves and  
160 ducting waves [Hayashi et al., 1981; Kim et al., 2010].

161

162 We further analyzed the propagation characteristics of Pc1 waves observed by CSES  
163 and SWARM satellites in the Northern and Southern hemispheres during the magnetic  
164 storm recovery phase. Firstly, we converted the magnetic field into field-aligned  
165 coordinates (FAC) and then applied polarization analysis according to the method of  
166 Means et al. [1972]. Figure 7, from top to bottom, shows SWARM magnetic field  
167 components in FAC (including perpendicular components  $B_r$  and  $B_a$  marked in blue  
168 and green, parallel component  $B_z$  marked in red), magnetic wave power spectrum in  
169 perpendicular direction and parallel direction, wave normal angle ( $0^\circ$  indicates parallel  
170 propagation and  $90^\circ$  indicates perpendicular propagation to the background magnetic  
171 field), ellipticity (positive indicates RHP and negative indicates LHP). For CSES, electric  
172 components in FAC, electric wave power spectrum in perpendicular direction and  
173 parallel direction, and field-aligned Poynting flux are also included in Figure 8-9.

174

175 It can be seen from the SWARM and CSES data in the Southern (Figure 7,8) and  
176 Northern hemispheres (Figure 9), the wave normal angles predominate below  $\sim 20^\circ$ ,  
177 indicating that Pc1 waves almost parallel propagate with the background magnetic  
178 field. Our result is somewhat different from the nightside observations in the  
179 ionosphere by Pisa et al. (2015) and Kim et al. (2018), which show the wave normal  
180 angles are scattered or have different tendency between two hemispheres. For CSES,  
181 based on the HPM and EFD data, we also calculate the field-aligned Poynting flux of  
182 Pc1 waves (shown by the blue lines in the bottom panels of Figure 8 and 9), which is  
183 positive in the Northern hemisphere, negative in the Southern hemisphere, indicating  
184 that Pc1 waves observed by CSES propagate along the background magnetic field  
185 downward into the ionosphere in the both hemispheres.

186

187 On the other hand, we find that the waves have dominant perpendicular power, and



188 the parallel power (compressional power) is almost zero, which means the waves are  
189 transverse. The transverse wave is one of the characteristics of the incident wave near  
190 the wave injection region [Engebretson et al.,2008; Kim et al., 2010]. The transverse  
191 wave also explains why the downward component in the local North-East-Down  
192 coordinates has the minimum wave power, as observed by satellites and ground  
193 stations (Figure 2-3, Figure 6). Near the injection region with a geomagnetic latitude  
194 of  $\sim 55^\circ$ , the dip angle of the geomagnetic field is about  $73^\circ$ . For a transverse wave, the  
195 power projected to the downward direction should be small. We further find the wave  
196 normal, electric field vector, background magnetic field are almost lie in the same  
197 plane (not shown here) with a deviation less than  $\pm 8^\circ$ , which proves that the incident  
198 transverse wave is Alfvénic.

199

200 And the ellipticity of Pc1 waves shows mixed polarization for the waves detected by  
201 CSES and SWARM in both hemispheres. To check whether our calculation results truly  
202 represent these wave properties, we also use Minimum and Maximum Variance  
203 Analysis (MVA) to get the MVA hodograph and the wave normal direction (not shown  
204 here), which are also consistent with current results. Therefore, it seems that all the  
205 Pc1 waves observed by CSES and SWARM have mixed ellipticities and propagate along  
206 the background magnetic field.

207

## 208 Discussion

209 In 1964, Wentworth et al. proposed that during storm recovery phase, the  
210 plasmopause expanding into the ring current region can excite EMIC wave. Through  
211 simulation, Horne and Thorne et al. [1993] found that the growth rate of EMIC wave  
212 inside the plasmopause is obviously lower than that outside the plasmopause, and its  
213 peak is near the plasmopause. Using the CLUSTER satellite data, Grison et al. [2013]  
214 observed a typical magnetospheric EMIC wave near the plasmopause at an  $L$  value of  
215 about 4.2. They also believe that the Pc1 wave is easy to occur in the night side region  
216 of the plasmopause and propagate along the magnetic field during the high years of  
217 solar wind activity.

218

219 To identify the source of the Pc1 waves observed by CSES and SWARM, we use the  
220 CCMC model [Pierrard et al., 2008] to obtain the variation of the position of the  
221 plasmopause during this magnetic storm on August 26, 2018 (as shown in Figure 10).  
222 Results show that the plasmopause moves outward at about UTC 23:00 on August 27,  
223 and the  $L$  value reaches about 3 near local time 02:00. The red asterisk denotes the  
224 position where Pc1 waves were observed by CSES. Moreover, based on the formula in  
225 Carpenter and Anderson [1992] (shown as equation 1), the position of the



226 plasmopause is estimated at about  $L=2.98$ . Therefore, we suggest that the possible  
227 sources of Pc1 waves are nearly located at the plasmopause, and this is consistent with  
228 previous studies, that the outward expansion of the plasmasphere into the ring current  
229 during the recovery phase of geomagnetic storms may generate EMIC waves, which  
230 propagate along the background magnetic field to the ionosphere, and be observed  
231 by multi-ground stations [Wentworth,1964; Cornwall et al., 1970; Russell & Thorne,  
232 1970].

$$233 \quad \hat{L}_{pp} = 5.6 - 0.46 \times \max_{-24,-4} K_p \quad (1)$$

234 According to the wave analysis performed using CSES and SWARM data, together with  
235 ground station observations, we suggest that the satellites are close to the wave  
236 injection regions in the Southern and northern hemisphere, during the recovery phase  
237 of the storm. The incident waves propagate almost along the background magnetic  
238 field, as transvers Alfvén waves, which has long been predicted by theoretical studies,  
239 although direct observations are rare. However, the ellipticity of the waves shows a  
240 complex pattern, which is different from the polarizations of EMIC waves (LHP) in the  
241 magnetosphere found by previous works [Fraser et al., 1975a, b; Erlandson et al.,  
242 1990]. Theoretical studies predict that EMIC waves triggered near the Earth's magnetic  
243 equator propagate toward the ionosphere, changing wave characteristics such as  
244 ellipticity and wave normal angle when they pass through multicomponent plasma  
245 [Denton, 2018; Johnson & Cheng, 1999; Kim & Johnson, 2016]. The mixed polarization  
246 pattern observed in our case might either result from incident waves with complex  
247 polarization pattern, or be attributed to the interference between the incident wave  
248 and ducting waves in the ionospheric waveguide.

249  
250 Joint magnetic field and electric field observations onboard CSES provide  
251 unambiguous evidence that Pc1 waves propagate downward into the ionosphere in  
252 the nearly conjugate ionospheric regions. Although the observations at north and  
253 south are temporally separated by about 30 mins, it seems reasonable to infer that  
254 the EMIC waves propagate northward and southward from the magnetic equatorial  
255 region simultaneously, and wave reflection from the ionosphere is insignificant. Our  
256 result is in accord with the CRRES satellite measurements reported by Loto'aniu et al.  
257 (2005), which observed that outside a region of about  $\pm 11^\circ$  MLAT around the equator,  
258 the Poynting vectors of the EMIC waves are directed away from the equator along the  
259 magnetic field lines.

260  
261 Pc1 waves sometimes have repetitive wave packet structures, which have been  
262 explained by a bouncing wave packet model [e.g., Jacobs and Watanabe, 1964].  
263 According to this model, a wave packet triggered in the equatorial region travels along



264 the magnetic field line, and is reflected between conjugate hemispheres. The Poynting  
265 vector is an important parameter for establishing the propagation direction of wave  
266 packet energy. CSES observations of Poynting vector in the ionospheric do not seem  
267 to support this model.

268

### 269 **Conclusion**

270 In this paper, using the simultaneous observations from CSES and SWARM satellites  
271 and the ground geomagnetic stations data, we investigated the typical Pc1 waves in  
272 the Northern and Southern ionospheric hemispheres. Our principal results are as  
273 follows.

274 1. During the storm recovery phase on Aug. 27, 2018, the typical Pc1 waves were  
275 recorded by the SGO stations on the ground for several hours. Meanwhile, the Pc1  
276 waves were detected by the China Seismo-Electromagnetic Satellite (CSES) and  
277 SWARM both in Northern and Southern hemispheres in the high latitude post-  
278 midnight ionosphere region with a central frequency about 2 Hz.

279

280 2. In the field-aligned coordinate system, the power spectrum, ellipticity and normal  
281 wave angle, Poynting vector are analyzed. Results show that the satellites observed  
282 transverse Alfvén waves with mixed polarizations, propagating almost parallel to the  
283 background magnetic field downward, which imply the satellites were close to the  
284 wave injection region in the ionosphere at about  $L=3$ . Attenuation of Pc1 wave power  
285 at ground stations with increasing distance from  $L=3$  also supports the idea that CSES  
286 observes the wave activities near the injection region.

287

288 3. Furthermore, it is also found that the position of the plasmopause calculated by  
289 CCMC model and equation of Carpenter and Anderson is almost at  $L=3$ . Therefore, we  
290 suggest the possible sources of waves are near the plasmopause, which is consistent  
291 with previous studies that the outward expansion of the plasmasphere into the ring  
292 current during the recovery phase of geomagnetic storms may generate  
293 electromagnetic ion cyclotron (EMIC) waves. Downward pointing Poynting fluxes  
294 measured by CSES at nearly conjugate hemispheres suggest EMIC waves propagate  
295 northward and southward simultaneously to the ionosphere at about  $L=3$ .

296

### 297 **Acknowledgments**

298 The work is supported by NSFC grant 41904147, National Key Research and  
299 Development Programs of Ministry of Science and Technology of the People's Republic  
300 of China (MOST) (2016YBF0501503, 2018YFC1503501). This research made use of the



301 data from CSES mission, a project funded by China National Space Administration  
302 (CNSA) and China Earthquake Administration (CEA). Additionally, thanks to ESA  
303 SWARM teams for providing SWARM FGM data, and SGO Webs for providing the SGO  
304 magnetic field data, and NASA CDA Web for providing the OMNI solar wind and  
305 magnetic field data, and NASA CMCC Web for providing the plasmopause simulation  
306 data.

307

## 308 Reference

309 Reference

310 Anderson, B. J., Takahashi, K., Erlandson, R. E., & Zanetti, L. J.: Pc1 pulsations observed  
311 by AMPTE/CCE in the Earth's outer magnetosphere, *Geophysical Research Letters*,  
312 17(11), 1853–1856, <https://doi.org/10.1029/gl017i011p01853>, 1990.

313 Anderson, B. J., & Hamilton, D. C.: Electromagnetic ion cyclotron waves stimulated by  
314 modest magnetospheric compressions, *Journal of Geophysical Research*, 98(A7),  
315 11369, <https://doi.org/10.1029/93ja00605>, 1993.

316 Anderson, B. J., Denton, R. E., Ho, G., Hamilton, D. C., Fuselier, S. A., and Strangeway,  
317 R. J.: Observational test of local proton cyclotron instability in the Earth's  
318 magnetosphere, *Journal of Geophysical Research: Space Physics*, 101(A10), 21527–  
319 21543, <https://doi.org/10.1029/96ja01251>, 1996.

320 Bortnik, J., Cutler, J. W., Dunson, C., Bleier, T. E., & McPherron, R. L.: Characteristics of  
321 low-latitude Pc1 pulsations during geomagnetic storms, *Journal of Geophysical*  
322 *Research: Space Physics*, 113(A4), n/a–n/a, <https://doi.org/10.1029/2007ja012867>,  
323 2008.

324 Bossen, M., McPherron, R. L., & Russell, C. T.: A statistical study of Pc 1 magnetic  
325 pulsations at synchronous orbit, *Journal of Geophysical Research*, 81(34), 6083–6091,  
326 <https://doi.org/10.1029/ja081i034p06083>, 1976.

327 Carpenter, D. L., & Anderson, R. R.: An ISEE/whistler model of equatorial electron  
328 density in the magnetosphere, *Journal of Geophysical Research*, 97(A2), 1097,  
329 <https://doi.org/10.1029/91ja01548>, 1992.

330 Cornwall, J. M.: Cyclotron instabilities and electromagnetic emission in the ultralow  
331 frequency and very low frequency ranges, *Journal of Geophysical Research*, 70(1), 61–  
332 69, <https://doi.org/10.1029/jz070i001p00061>, 1965.

333 Denton, R. E.: Electromagnetic Ion Cyclotron Wave fields in a Realistic Dipole Field,  
334 *Journal of Geophysical Research: Space Physics*, 123(2), 1208–1223,  
335 <https://doi.org/10.1002/2017ja024886>, 2018.

336 Engebretson, M. J., Posch, J. L., Westerman, A. M., Otto, N. J., Slavin, J. A., Le, G.,  
337 Strangeway, R. J. and Lessard, M. R.: Temporal and spatial characteristics of Pc1 waves  
338 observed by ST5, *Journal of Geophysical Research: Space Physics*, 113(A7), n/a–n/a,



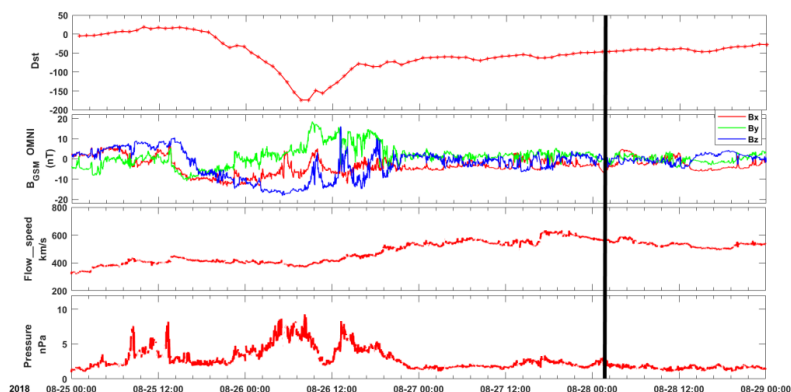
- 339 <https://doi.org/10.1029/2008ja013145>, 2008.
- 340 Erlanson, R. E., Aggson, T. L., Hoge, W. R., & Slavin, J. A.: Simultaneous observations  
341 of subauroral electron temperature enhancements and electromagnetic ion cyclotron  
342 waves, *Geophysical Research Letters*, 20(16), 1723–1726,  
343 <https://doi.org/10.1029/93gl01975>, 1993.
- 344 Fraser, B. J.: Polarization of Pc 1 pulsations at high and middle latitudes, *Journal of*  
345 *Geophysical Research*, 80(19), 2797–2807, doi:10.1029/ja080i019p02797, 1975a.
- 346 Fraser, B. J.: Ionospheric duct propagation and Pc 1 pulsation sources, *Journal of*  
347 *Geophysical Research*, 80(19), 2790–2796, <https://doi.org/10.1029/ja080i019p02790>,  
348 1975b.
- 349 Fujita, S., and Tamao, T.: Duct propagation of hydromagnetic waves in the upper  
350 ionosphere, 1, *Electromagnetic field disturbances in high latitudes associated with*  
351 *localized incidence of a shear Alfvén wave. Journal of Geophysical Research*, 93(A12),  
352 14665. <https://doi.org/10.1029/ja093ia12p14665>, 1988.
- 353 Grison, B., Santolík, O., Cornilleau-Wehrin, N., Masson, A., Engebretson, M. J., Pickett,  
354 J. S., Omura, Y., Robert, P. and Nomura, R.: EMIC triggered chorus emissions in Cluster  
355 data, *Journal of Geophysical Research: Space Physics*, 118(3), 1159–1169,  
356 <https://doi.org/10.1002/jgra.50178>, 2013.
- 357 Horne, R. B., & Thorne, R. M.: On the preferred source location for the convective  
358 amplification of ion cyclotron waves, *Journal of Geophysical Research*, 98(A6), 9233,  
359 <https://doi.org/10.1029/92ja02972>, 1993.
- 360 Johnson, J. R., & Cheng, C. Z.: Can Ion Cyclotron Waves Propagate to the Ground?  
361 *Geophysical Research Letters*, 26(6), 671–674, <https://doi.org/10.1029/1999gl900074>,  
362 1999.
- 363 Lin, R. L., Zhang, J. C., Allen, R. C., Kistler, L. M., Mouikis, C. G., Gong, J. C., Liu, L. Q.,  
364 Klecker, B., Sauvaud, J. A., Dunlop, M. W.: Testing linear theory of EMIC waves in the  
365 inner magnetosphere: Cluster observations, *Journal of Geophysical Research: Space*  
366 *Physics*, 119(2), 1004–1027, <http://doi.org/10.1002/2013ja019541>, 2014.
- 367 Hayashi, K., Kokubun, S., Oguti, T., Tsuruda, K., Machida, S., Kitamura, T., Saka, O.,  
368 Watanabe, T.: The extent of Pc 1 source region in high latitudes, *Canadian Journal of*  
369 *Physics*, 59(8), 1097–1105, <https://doi.org/10.1139/p81-145>, 1981.
- 370 Huang, J., Lei, J., Li, S., Zeren, Z., Li, C., Zhu, X., Yu, W.: The Electric Field Detector (EFD)  
371 onboard the ZH-1 satellite and first observational results, *Earth and Planetary Physics*,  
372 2(6), 469–478, <https://doi.org/10.26464/epp2018045>, 2018.
- 373 Iyemori, T., and Hayashi, K.: PC 1 micropulsations observed by Magsat in the  
374 ionospheric F region, *Journal of Geophysical Research*, 94(A1), 93,  
375 <https://doi.org/10.1029/ja094ia01p00093>, 1989.
- 376 Jacobs, J.A., Watanabe, T.: Micropulsation whistlers, *Journal of Atmospheric and*



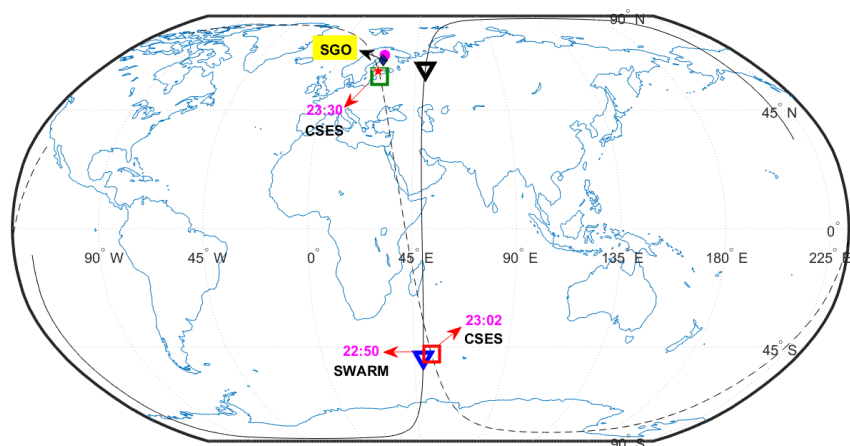
- 377 Terrestrial Physics 26, 825–829, 1964.
- 378 Kim, H., Lessard, M. R., Engebretson, M. J., Lühr, H.: Ducting characteristics of Pc 1  
379 waves at high latitudes on the ground and in space, *Journal of Geophysical Research:*  
380 *Space Physics*, 115(A9), n/a–n/a, <https://doi.org/10.1029/2010ja015323>, 2010.
- 381 Kim, E.-H., and Johnson, J. R.: Full-wave modeling of EMIC waves near the He+  
382 gyrofrequency, *Geophysical Research Letters*, 43(1), 13–21,  
383 <https://doi.org/10.1002/2015gl066978>, 2016.
- 384 Kim, H., Hwang, J., Park, J., Bortnik, J., Lee, J.: Global characteristics of electromagnetic  
385 ion cyclotron waves deduced from Swarm satellites, *Journal of Geophysical Research:*  
386 *Space Physics*, 123, 1325–1336, <https://doi.org/10.1002/2017JA024888>, 2018.
- 387 Loto'aniu, T. M.: Propagation of electromagnetic ion cyclotron wave energy in the  
388 magnetosphere., *Journal of Geophysical Research*, 110(A7).  
389 <https://doi.org/10.1029/2004ja010816>, 2005.
- 390 Lysak, R. L: Propagation of Alfvén waves through the ionosphere: Dependence on  
391 ionospheric parameters, *J. Geophys. Res.*, 104, 10,017, 1999.
- 392 McCollough, J. P., Elkington, S. R., Usanova, M. E., Mann, I. R., Baker, D. N., Kale, Z. C.:  
393 Physical mechanisms of compressional EMIC wave growth, *Journal of Geophysical*  
394 *Research: Space Physics*, 115(A10), n/a–n/a, <https://doi.org/10.1029/2010ja015393>,  
395 2010.
- 396 Means, J. D.: Use of the three-dimensional covariance matrix in analyzing the  
397 polarization properties of plane waves, *Journal of Geophysical Research*, 77(28), 5551–  
398 5559, <https://doi.org/10.1029/ja077i028p05551>, 1972.
- 399 Olson, J. V., & Lee, L. C.: Pc1 wave generation by sudden impulses, *Planetary and Space*  
400 *Science*, 31(3), 295–302, [https://doi.org/10.1016/0032-0633\(83\)90079-x](https://doi.org/10.1016/0032-0633(83)90079-x), 1983.
- 401 Park, J., Lühr, H., and Rauberg, J.: Global characteristics of Pc1 magnetic pulsations  
402 during solar cycle 23 deduced from CHAMP data, *Annales de Geophysique*, 31(9),  
403 1507–1520, <https://doi.org/10.5194/angeo-31-1507-2013>, 2013.
- 404 Pierrard, V., and Stegen: A three-dimensional dynamic kinetic model of the  
405 plasmasphere, *J. Geophys. Res.*, 113, A10209, <https://doi.org/10.1029/2008JA013060>,  
406 2008.
- 407 Píša, D., Parrot, M., Santolík, O. and Menietti, J. D.: EMIC waves observed by the low-  
408 altitude satellite DEMETER during the November 2004 magnetic storm, *J. Geophys.*  
409 *Res. Space Physics*, 120, 5455–5464, <https://doi.org/10.1002/2014JA020233>, 2015.
- 410 Russell, C. T., & Thorne, R. M.: STRUCTURE OF THE INNER MAGNETOSPHERE, Univ. of  
411 California, Los Angeles, 1970.
- 412 Usanova, M. E., Mann, I. R., Bortnik, J., Shao, L., Angelopoulos, V.: THEMIS observations  
413 of electromagnetic ion cyclotron wave occurrence: Dependence on AE, SYMH, and  
414 solar wind dynamic pressure, *Journal of Geophysical Research: Space Physics*,



415 117(A10), n/a–n/a, <https://doi.org/10.1029/2012ja018049>, 2012.  
416 Wentworth, R. C.: Enhancement of hydromagnetic emissions after geomagnetic  
417 storms, *J. Geophys. Res.*, 69(11), 2291–2298, doi:10.1029/JZ069i011p02291, 1964.  
418 Zhou, B., Yang, Y. Y., Zhang, Y. T., Gou, X. C., Cheng, B. J., Wang, J. D., and Li, L.: Magnetic  
419 field data processing methods of the China Seismo-Electromagnetic Satellite, *Earth*  
420 *Planet. Phys.*, 2(6), 455–461, <https://doi.org/10.26464/epp2018043>, 2018.  
421 Zhou, B., Cheng, B. J., Gou, X.C., Li, L., Zhang, Y. T., Wang, J. D., Magnes, W., Lammegger,  
422 R., Pollinger, A., Ellmeier, M., Xiao, Q., Zhu, X. H., Yua, S. G., Yang, Y. Y. and Shen, X. H.:  
423 First in-orbit results of the vector magnetic field measurement of the High Precision  
424 Magnetometer onboard the China Seismo-Electromagnetic Satellite, *Earth Planets*  
425 *Space* 71, 119, <https://doi.org/10.1186/s40623-019-1098-3>, 2019.  
426



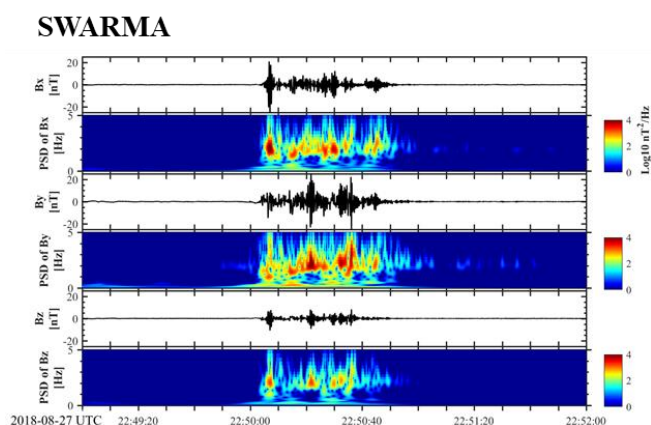
427  
428 Figure 1. The solar wind conditions and geomagnetic index from Aug. 25 to 29, 2018.  
429 From top to bottom: Dst index, interplanetary magnetic field, solar wind speed and  
430 solar wind dynamic pressure, respectively. The occurrence of Pc1 waves is marked by  
431 the black line.



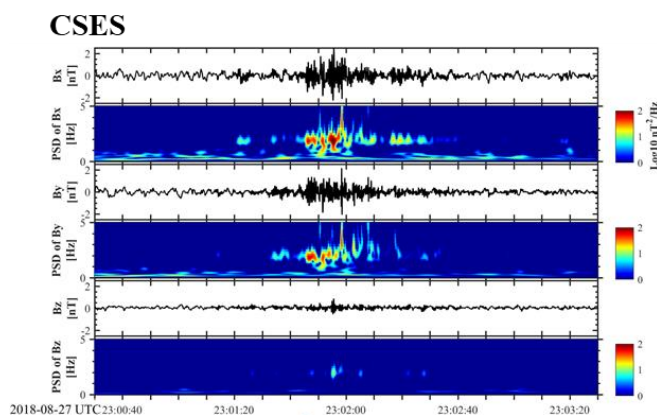
432



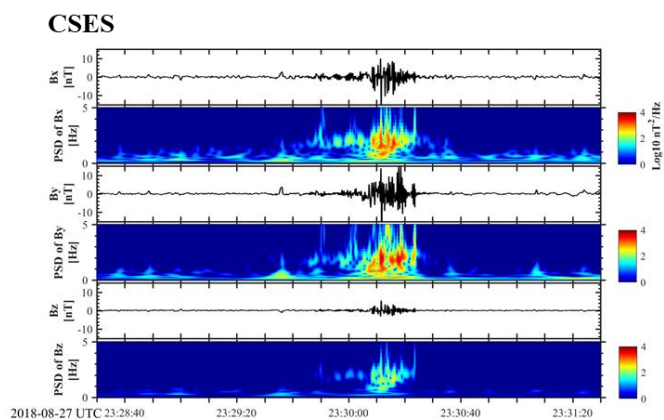
433 Figure 2. The locations of Pc1 waves observed by CSES (squares) and SWARM (triangles)  
434 satellites. The pentagram, rhombus and circle represent three the SGO stations:  
435 Nurmijärvi (NUR;  $L = 3.4$ ,  $57.1^\circ\text{N}$ ,  $101.2^\circ\text{E}$ , QD), Oulu (OUL;  $L = 4.5$ ,  $61.9^\circ\text{N}$ ,  $104.1^\circ\text{E}$ ,  
436 QD), and Sodankylä (SOD;  $L = 5.3$ ,  $64.3^\circ\text{N}$ ,  $105.6^\circ\text{E}$ , QD), respectively. The black dotted  
437 and solid lines denote the trajectories of CSES and SWARMA satellites, respectively  
438 and the red arrows represents three Pc1 wave observations.



439  
440 Figure 3. The power spectral densities (PSDs) of the magnetic fields during the Pc1  
441 wave period (UTC 22:50-22:51) observed by SWARM-A.



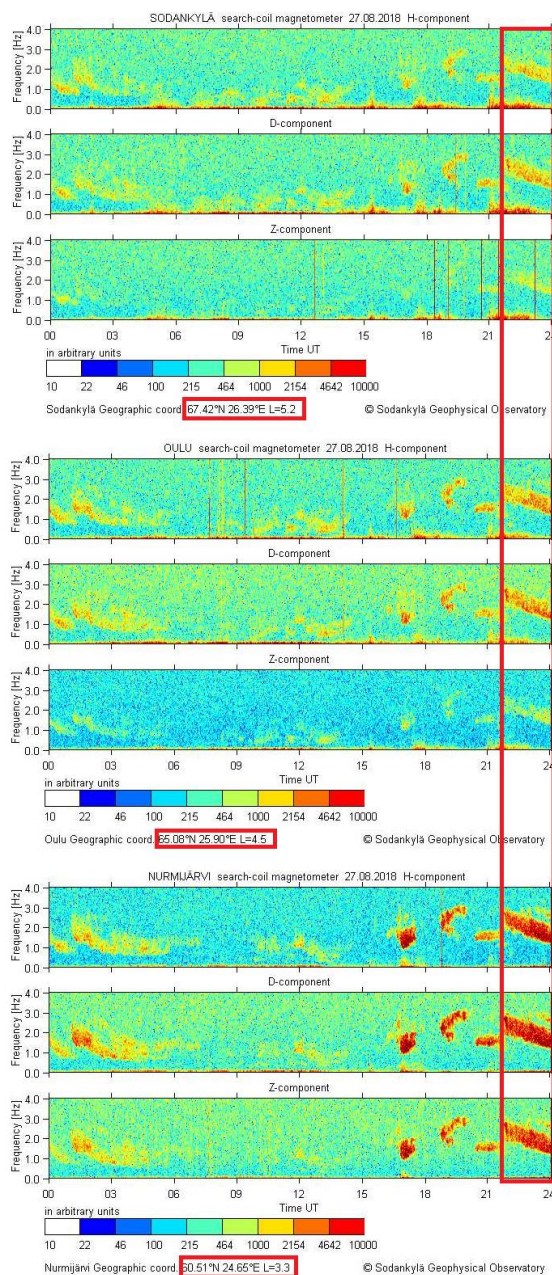
442  
443 Figure 4. The power spectral densities (PSDs) of the magnetic fields during the Pc1  
444 wave period (UTC 23:01-23:02) observed by CSES.



445

446 Figure 5. The power spectral densities (PSDs) of the magnetic fields during the Pc1

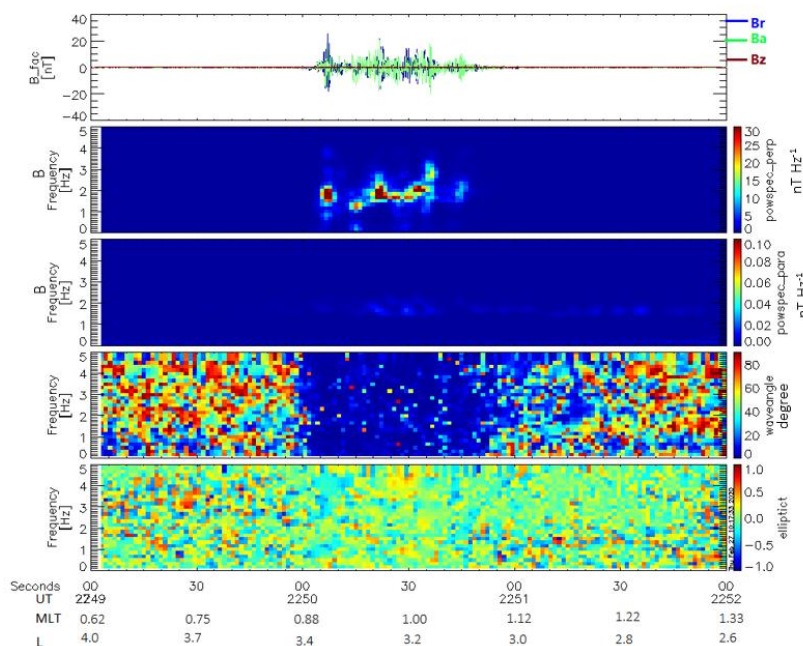
447 wave period (UTC 23:30-23:31) observed by CSES.



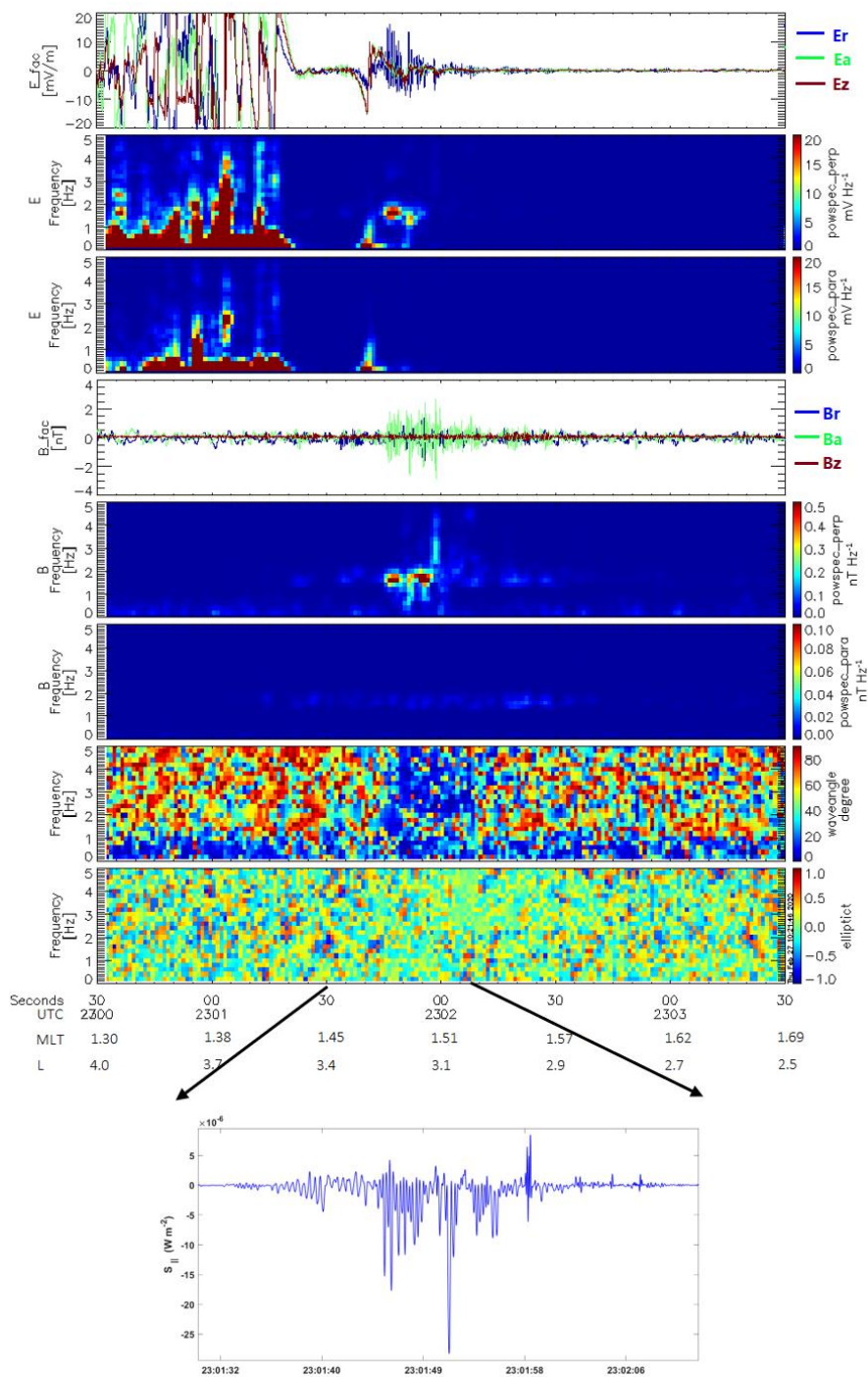
448

449 Figure 6. The power spectral densities (PSDs) of the magnetic fields during the Pc1  
450 wave period (UTC 22:00-24:00) observed by SGO ground stations at different  $L$  shell  
451 values.

452



453  
 454 Figure 7. The wave propagation and polarization features of the Pc1 waves observed  
 455 by SWARM. From top to bottom, magnetic field components (including perpendicular  
 456 components Ba and Br marked in blue and green, parallel component Bz marked in  
 457 red), wave power spectrum in perpendicular and parallel directions, wave normal  
 458 angle and ellipticity computed by wave vector analysis of Means [1972]. (positive  
 459 indicates right-handed polarization and negative indicates left-handed).

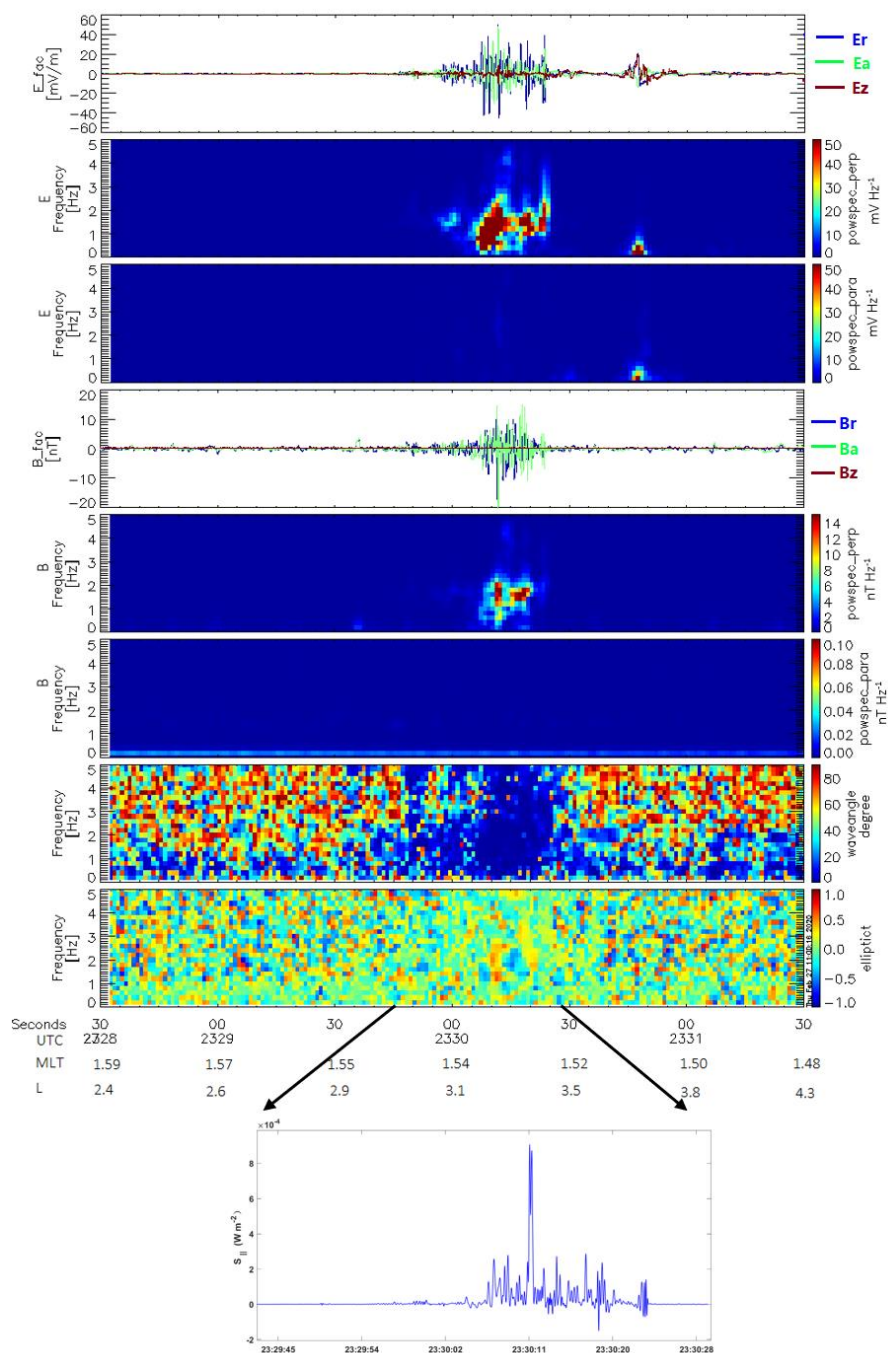


460

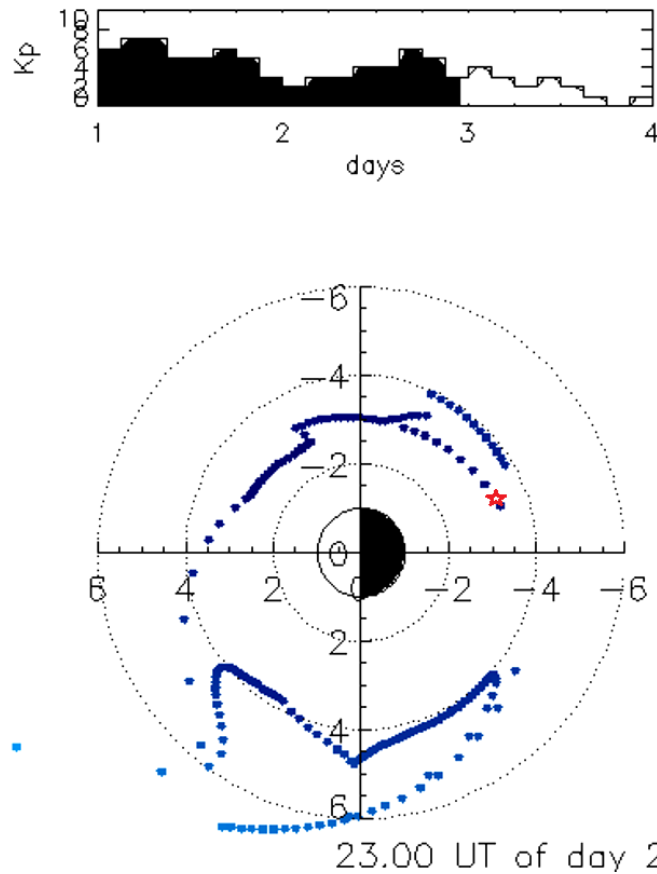
461 Figure 8. The wave propagation and polarization features of the Pc1 waves observed



462 by CSES in the Southern hemisphere. From top to bottom, electric field components  
463 (including perpendicular components  $E_a$  and  $E_r$  marked in blue and green, parallel  
464 component  $E_z$  marked in red), electric wave power spectrum in perpendicular and  
465 parallel directions; magnetic field components (including perpendicular components  
466  $B_a$  and  $B_r$  marked in blue and green, parallel component  $B_z$  marked in red), wave  
467 power spectrum in perpendicular and parallel directions, magnetic wave normal angle  
468 and ellipticity, the field-aligned Poynting fluxes.



469  
 470 Figure 9. The wave propagation and polarization features of the Pc1 waves observed  
 471 by CSES in the Northern hemisphere, same format as Figure 8.  
 472



473  
474 Figure 10. The Kp index (upper) and the simulated plasmopause location (lower)  
475 marked by blue dots at UTC 23:00 on August 27, 2018 from CCMC Web. The asterisk  
476 represents the conjugate location of Pc1 waves observed by CSES in the Southern  
477 hemisphere.